



Cite this: *Phys. Chem. Chem. Phys.*,
2015, 17, 9040

NEXAFS and XPS studies of nitrosyl chloride

Luca Schio,^a Cui Li,^{bc} Susanna Monti,^{db} Peter Salén,^e Vasylyatsyna,^f Raimund Feifel,^f Michele Alagia,^g Robert Richter,^h Stefano Falcinelli,ⁱ Stefano Stranges,^{ig} Vitali Zhaunerchyk^{*f} and Vincenzo Carravetta^{*c}

The electronic structure of nitrosyl chloride (ClNO) has been investigated in the gas phase by X-ray Photoelectron (XPS) and Near Edge X-ray Absorption Fine Structure (NEXAFS) spectroscopy at the Cl 2p, Cl 2s, N 1s and O 1s edges in a combined experimental and theoretical study. The theoretical calculations at different levels of approximation predict ionization potential values in good agreement with the experimental data and allow us to assign the main features of the absorption spectra. An unexpected failure of the density functional model is, however, observed in the calculation of the Cl 2s binding energy, which is related to a large self-interaction error. Largely different photoabsorption cross-section patterns are experimentally observed in core excitations from the investigated quantum shells ($n = 1, 2$). This finding is confirmed by the oscillator strength distributions calculated at different absorption edges; in the case of the $n = 2$ shell the bands below the threshold are extremely weak and most of the absorption intensity is due to excitations in the continuum.

Received 16th December 2014,
Accepted 16th February 2015

DOI: 10.1039/c4cp05896h

www.rsc.org/pccp

1 Introduction

Chlorine-bearing molecules are present in the terrestrial atmosphere as side products of human activities and represent severe air pollutants. In particular, they can efficiently be photolyzed by ultraviolet (UV) radiation, releasing atomic chlorine radicals which are harmful for the ozone layer. The depletion of the latter can have drastic effects on life on Earth. Chlorine compounds can also occur naturally in the atmosphere. One such compound is ClNO that can be produced in the marine areas from sea salts by ocean wind-generated waves (see, e.g., ref. 1 and 2). Similarly to other chlorine-bearing molecules, ClNO becomes a potential source of chlorine free

radicals when it reaches the upper atmosphere of Earth and undergoes photolysis.

ClNO in the ground state is bent and has the C_s symmetry. The equilibrium geometry is characterized by a Cl–N–O bond angle of 113.3° and bond lengths of $r_{\text{ClN}} = 1.97 \text{ \AA}$ and $r_{\text{NO}} = 1.14 \text{ \AA}$.³ The valence electronic structure of ClNO was investigated in early studies by photoelectron spectroscopy and molecular orbital (MO) calculations.^{4–6} The ClNO electronic configuration of the frontier MOs is... $(3a'')^2(12a')^2(13a')^2(4a'')^0(14a')^0\dots$,⁷ where single prime and double prime denote orbitals that are symmetric and anti-symmetric with regard to the molecular plane, respectively. It was concluded that the first observed structure in the valence photoelectron spectrum, made of three overlapping bands, is associated with the electron removal from the three highest occupied MOs (HOMOs): HOMO ($13a'$), HOMO – 1 ($12a'$) and HOMO – 2 ($3a''$), of very similar energies and almost pure Cl nonbonding character. Partially resolved vibronic structure also suggested that the HOMO has a weak Cl–N bonding character, because of the ν_2 values (Cl–N bond stretching) decrease upon ionization.⁵

In more recent studies the photolysis reactions of ClNO have extensively been investigated both theoretically and experimentally in the UV-visible spectral range.^{8–14} In particular, in the photon energy range of 4–7 eV such investigations revealed a strong broad absorption band consisting of three contributions, the most intense of which has a maximum at 6.3 eV and is associated with the formation of the $4^1A'$ excited state.^{8,9,11,13} $4^1A'$ was assigned to electron excitation from the HOMO to the lowest unoccupied MO + 1 (LUMO + 1) ($14a'$).^{8,9} This latter MO

^a Dipartimento di Chimica, Università Sapienza, Roma, I-00185, Italy

^b Theoretical Chemistry and Biology, School of Biotechnology, Royal Institute of Technology, 10044 Stockholm, Sweden

^c CNR-IPCF, Institute of Chemical Physical Processes, via G. Moruzzi 1, I-56124 Pisa, Italy. E-mail: carravetta@ipcf.cnr.it

^d CNR-ICCOM, Institute of Chemistry of Organometallic Compounds, via G. Moruzzi 1, I-56124 Pisa, Italy

^e Department of Physics, Stockholm University, 106 91 Stockholm, Sweden

^f Department of Physics, University of Gothenburg, 412 96 Gothenburg, Sweden. E-mail: vitali.zhaunerchyk@physics.gu.se

^g IOM-CNR Tasc, SS-14, Km 163.5 Area Science Park, Basovizza, I-34149 Trieste, Italy

^h Elettra – Sincrotrone Trieste, Area Science Park, 34149 Basovizza, Trieste, Italy

ⁱ Dipartimento di Ingegneria Civile ed Ambientale, Università di Perugia, 06125 Perugia, Italy

^j Dipartimento di Chimica e Tecnologie del Farmaco, Università Sapienza, Roma, I-00185, Italy

has a strong antibonding π_{NO}^* character and corresponds in the isolated NO molecule to the degenerate in-plane (xy) π^* MO that is mixed with the Cl $3p_x$ atomic orbital (where y is the NO bond axis). The mixing is such that the LUMO + 1 has also a nonbonding σ_{ClNO}^* character. As for the other two contributions to the broad band, the one corresponding to the excited states $3^1A'^{8,9,11,13}$ was ascribed to electron excitation from the HOMO – 1 ($12a'$) to the LUMO + 1 ($14a'$),^{8,9} whilst the assignment for the third component is controversial.^{8,9,11,13} Absorption features at lower energies (2–3.8 eV) are due to electron excitations from the three Cl nonbonding MOs, $13a'$, $12a'$ and $3a''$, to the LUMO ($4a''$), of antibonding π_{NO}^* character and perpendicular to the molecular plane, and to the LUMO + 1.^{8,9} It is worth noting that the LUMO and the LUMO + 1 are computed to be rather low energy MOs of π_{NO}^* character.^{8,9} Excitations to virtual MOs of σ_{NO}^* character are not observed in the experimental energy range investigated, since MOs of this character should have energies higher than that of LUMO + 1.

Although UV-visible absorption and valence electron ionization processes of ClNO are hitherto well studied, to the best of our knowledge, only a few investigations were performed at higher photon energies⁶ and no systematic studies involving core levels have been carried out. Near-Edge X-ray Absorption Fine Structure (NEXAFS) spectroscopy is a powerful tool to characterize the electronic structure of molecular systems containing light atoms, both as isolated species in the gas phase or on surfaces, because (1) it is an element specific spectroscopy as X-ray absorption edges of different elements have different energies, and (2) it is also very sensitive to the local chemical environment of the absorbing atom.¹⁵ NEXAFS spectroscopy implies excitation of an inner-shell electron to an unoccupied (virtual) MO which is destabilized by Auger electron emission occurring on the femtosecond timescale. The core-hole lifetime broadening is typically of a few hundred meV; unresolved vibronic structures can also contribute significantly to the width of the absorption band. Nowadays NEXAFS spectra can be investigated both theoretically and experimentally, in the latter case at high photon energy resolution. Experimentally, NEXAFS spectroscopy is usually performed using synchrotron light sources which provide monochromatic, tunable, and high-flux X-ray radiation in a wide energy range. Thanks to its small size, a variety of atomic species and sufficient structural complexity, ClNO also provides a convenient polyatomic system for theoretical and experimental studies of inner shell electron excitation from different quantum shells, namely $n = 1$ (O 1s and N 1s) and $n = 2$ (Cl 2s and Cl 2p). Furthermore, the molecular small size enables a variety of theoretical methods to be applied and by comparing with experimental data gaining some physical insights into the capabilities of different methods.

In this work we present NEXAFS spectra of ClNO recorded in the vicinity of the Cl 2p, Cl 2s, N 1s, and O 1s edges as well as results of theoretical simulations to assign various spectral features. We also report the theoretically predicted and experimentally measured Cl 2p, Cl 2s, N 1s, and O 1s Ionization Potentials (IPs) of ClNO, which to our knowledge are hitherto unknown. The experimental IP values were obtained by X-ray

Photoelectron Spectroscopy (XPS). A number of theoretical methods have been, in fact, applied, namely Hartree–Fock (HF), Density Functional Theory (DFT) and Multi Configuration Self Consistent Field (MCSCF), and their different capabilities are discussed by comparison of the calculated results with the experiment.

2 Experimental procedure

2.1 Sample preparation

High purity ClNO was prepared by the direct combination of pure NO and Cl₂ gases according to the reaction scheme $2\text{NO} + \text{Cl}_2 \rightarrow 2\text{ClNO}$. Care was taken in the sample handling since ClNO is very toxic and chemically highly reactive, being extremely corrosive, especially in the presence of water, like the reactant gases NO and Cl₂. The reactants were admitted in the manifold vacuum line from the tanks by means of stainless needle valves and pipes. The gas regulators and pressure gauges (MKS Baratron pressure transducer) used in the synthesis are made of special corrosion-resistant alloys. The reaction vessels and the vacuum manifold, made of pyrex and equipped with teflon stopcocks, were pumped down and heated for one hour while pumping. The whole apparatus was thoroughly flushed with pure helium and then evacuated. This procedure was repeated three times in order to remove all moisture from internal surfaces. Stoichiometric quantities of the reactant gases Cl₂ and NO were accurately measured separately by means of two equal pyrex bulbs (6.0 L volume), and by setting the desired gas pressures. The glass inner surfaces of the two bulbs were pre-treated (heating-pumping and prolonged exposure to the reactant gas) before filling them with Cl₂ and NO. The whole apparatus was protected with Al foils from light exposure to prevent decomposition by photolysis of the ClNO product. After mixing the reactants, the reaction progress was monitored by the gas pressure drop. After 40 minutes reaction at room temperature, the gaseous mixture was fully condensed at the liquid nitrogen temperature in one of the two bulbs where it was left for warming up at room temperature and kept for about three hours. Finally, the ClNO sample was transferred by liquid nitrogen trapping in a small glass bulb equipped with a teflon stopcock. The liquid ClNO sample was stored at low temperature (–20 °C) for several weeks. Before the experiment the ClNO sample was purified and checked by the following procedure. The liquid ClNO was kept at low temperature (–55 °C) in an EtOH thermostatic bath. A teflon membrane pump, with 6 torr input pressure, was used to pump over the liquid ClNO for about 40 minutes to remove a small part of it. NO and Cl₂ gases, possibly present as traces in the ClNO sample, were thus preferentially removed as NO and Cl₂ have substantially higher vapor pressure than ClNO at $T = -55$ °C. At this temperature, in fact, ClNO and Cl₂ have 55 torr and 342 torr vapor pressure,^{16,17} respectively, while NO is much more volatile as its critical temperature and pressure are –93 °C and 64.8 bar.¹⁷ The ClNO purity was checked by recording the HeI UV photoelectron spectrum (UPS) using an angle-resolved photoelectron spectrometer specifically designed for synchrotron radiation investigations of highly reactive and

short-lived species.¹⁸ The obtained photoelectron spectrum did not show the characteristic features of NO, Cl₂, or Cl, and was in excellent agreement with the published ClNO HeI UPS recorded previously in the gas phase.⁵

2.2 XPS and NEXAFS measurements

The XPS and NEXAFS spectra of ClNO have been recorded at the Gas Phase beam line of the Elettra synchrotron facility located in Trieste, Italy.¹⁹ The beamline is equipped with a high-flux undulator and a high-resolution soft X-ray monochromator with resolving power better than 10 000. The beam line allows a continuous photon energy scan by varying the angles of the monochromator grating and the plane mirror, and suitably tuning the undulator gap. The vapor sample was injected through a hypodermic needle and rated by a needle valve, both made of stainless steel. Traces of NO were always detected in the spectra due to the decomposition of ClNO on the metal surfaces along the sample inlet system.

The Cl 2p, Cl 2s, N 1s, and O 1s XPS spectra of ClNO were recorded using a 150 mm mid-radius hemispherical VG electron analyzer mounted at the magic angle of 54.7° with respect to the polarization plane of radiation. The spectra were energy calibrated by introducing separately in the ionization chamber a small amount of N₂, CO₂, and CHCl₃ gases simultaneously with the sample, and referring the observed ClNO features to the calibration peak of a known IP.^{20–23} The ClNO components were easily distinguished from the calibration peaks by recording spectra at constant sample pressure and different partial pressures of the calibration gas. The monochromator photon bandpass and the analyzer pass energy were chosen depending on the desired ClNO signal level. The Cl 2p, Cl 2s, N 1s, and O 1s XPS spectra were recorded at the photon energies of 255 eV, 350 eV, 495 eV, and 628 eV, respectively. These energies were chosen as the best compromise to obtain large photoionization cross section (close to threshold) and modest band shape deformation caused by the post-collisional interaction effect (far above threshold). The analyzer resolution was set at ≈0.2 eV for the O 1s, N 1s and Cl 2s spectra (10 eV pass energy), while for the Cl 2p XPS the resolution was about 0.1 eV (5 eV pass energy).

The NEXAFS spectra were measured by scanning the soft X-ray energy and monitoring the total ion yield by a Multi-Channel Plate (MCP, Hamamatsu) detector. The ion yield detection mode was preferred over the total electron yield mode since the experimental setup easily allows ion detection to be performed over the whole solid angle of photoemission, whilst this is not achievable for the electron detection. In order to take into account the change in photon flux at different photon energies, which is related to the optical transmission of the beam line, the photon flux was monitored simultaneously with the total ion signal using a photodiode. The normalized NEXAFS spectra were finally obtained as the ratio of the MCP total ion and photodiode signals. The NEXAFS spectra for nitrosyl chloride were recorded in the vicinity of the N K-edge, the O K-edge and the Cl L-edge; the Cl K-edge spectrum was not recorded since the ionization energy of the Cl 1s goes beyond the spectral range of the beam line.⁶ To calibrate the photon energy

of the recorded resonances, separate NEXAFS measurements were also performed for N₂, CO₂, and Ar which have NEXAFS spectra in similar energy ranges^{24–26} as the pre-edge N 1s, O 1s, Cl 2s and Cl 2p resonances in ClNO, respectively.

3 Computational details

The molecular geometry of the ClNO molecule was optimized using GAMESS,²⁷ by HF calculations with the TZV²⁸ basis set. The geometry thus obtained, namely a Cl–N–O bond angle of 113.4° and bond lengths of $r_{\text{ClN}} = 1.97 \text{ \AA}$ and $r_{\text{NO}} = 1.14 \text{ \AA}$, is in excellent agreement with the experimental values mentioned above.³ The IPs at the Cl L-edges, N K-edge, and O K-edge were computed by Δ HF calculation using the program DALTON (2013 version).²⁹ This approximation fully includes the effect of the electronic relaxation around the hole, but neglects the electron correlation. This latter quantity is about one order of magnitude smaller than the relaxation for a K-edge ionization, while in the case of the L-edges the electron correlation may, in principle, be equally important. For this reason we also considered Δ DFT calculations because the DFT method is generally believed to include, at least partially, electron correlation effects. The Δ DFT IP values as well as the NEXAFS spectra of ClNO considered at the different edges were computed using DEMON (StoBe version)³⁰ in the DFT transition state approximation. The IGLO-III orbital basis set,³¹ augmented by a large set of diffuse Gaussians centered on the excitation site,³² was adopted for all three types of atoms. The calculations were performed using two kinds of exchange–correlation functionals: BE88 + PD86 (the GGA exchange functional of Beck³³ and the correlation functional of Perdew³⁴) and PBE + PBE (the GGA exchange and correlation functionals of Perdew–Burke–Ernzerhof³⁵). Core excited states below the ionization threshold exhibit a “quasi-bound” character, and the computed values, both for the excitation energy and the intensity, generally show a relatively weak dependence on good quality basis sets. However, this is not the case for excited states above threshold, where the analysis of the intensity distribution should be performed more accurately by a procedure like Stieltjes imaging.^{36,37}

The DFT method in the transition moment approximation was proven to provide accurate NEXAFS spectra at K-edges^{38,39} but no studies, to our best knowledge, are available on the L-edges. Our Δ DFT calculations show, as will be discussed in the following section, quite poor results for the Cl 2s IP. In order to include electron correlation effects in a more reliable way more computational demanding higher level theoretical methods, such as MCSCF⁴⁰ and MRCI⁴¹ (Multi Reference Configuration Interaction), can be used. Here, the better performance of the Δ MCSCF method in predicting the Cl 2s IP was checked by us also for other Cl containing molecules (Cl₂CH₂ and ClCH₃). The deviation of the Δ MCSCF values compared to the experimental ones⁴² is, on average, only ±0.5 eV, while the values predicted by Δ DFT calculations are, as well as for ClNO, of several eV.

4 Results and discussion

4.1 XPS data and IP values

The experimental XPS spectra recorded at the photon energies of 255 eV, 350 eV, 495 eV and 628 eV are shown in Fig. 1(a)–(d), respectively. The calibrated XPS spectra allowed us to determine the IP values of ClNO as $\text{IP}(\text{Cl } 2p_{3/2}) = 205.40$ eV, $\text{IP}(\text{Cl } 2p_{1/2}) = 206.94$, $\text{IP}(\text{Cl } 2s) = 276.6$ eV, $\text{IP}(\text{N } 1s) = 411.3$ eV and $\text{IP}(\text{O } 1s) = 542.9$ eV. The observed widths of the XPS peaks, as full width at half maximum, are 1.0 eV for $\text{Cl}(2p_{3/2}$ and $2p_{1/2})$, 2.15 eV for $\text{Cl } 2s$, 0.42 eV for $\text{N } 1s$, and 1.23 eV for $\text{O } 1s$, whereas the values of the estimated instrumental broadening for the same peaks are 0.14 eV, 0.54 eV, 0.32 eV, and 0.40 eV, respectively. The other contributions to the observed width are the core-hole lifetime and the unresolved vibrational structure. Although the goal of the present XPS investigation is to measure the vertical IPs, rather than a fine analysis of the ionization peaks, it should be noted that taking into account the typical lifetime widths of the $\text{O } 1s$ (171–162 meV),^{43–45} $\text{N } 1s$ (130–102 meV)^{43,46,47} and $\text{Cl } 2p$ (100–81 meV)⁴³ core-holes, the vibrational broadening is quite significant in the core ionization of the terminal atoms O and Cl, whilst it is relatively much less important for the central atom N. Consequently, the equilibrium geometry change upon $\text{N } 1s$ ionization should not be dramatic. This consideration is supported by DFT geometry optimization calculations for the neutral ground state and the $\text{N } 1s$ and $\text{O } 1s$ core ionized states of ClNO. Such calculations show that the $\text{N } 1s$ and $\text{O } 1s$ ionized state geometries involve an increase in both bond lengths and angle. The variation is approximately 3% for the $\text{N } 1s$ ionic state, while for the $\text{O } 1s$ state we find the same percentage of elongation of the N–Cl bond, almost no variation in the angle, but a lengthening of as much as 5% for the N–O bond. The larger width of the $\text{O } 1s$ XPS band may thus be attributed to a larger activation of vibrational modes involving the N–O bond. The much larger broadening observed for the $\text{Cl } 2s$ ionization, 2.15 eV, is instead due to the very short lifetime of this

core-hole associated with the rapid Coster–Kronig electronic decay processes $\text{Cl } 2s \leftarrow 2p$.

The XPS spectra exhibit the expected main photoelectron bands as well as other weak peaks. Most of these weak peaks are due to core ionized residual gases desorbing from the inner surfaces of the chamber and the sample inlet system, or decomposition and secondary reaction products of ClNO molecules, like the HCl^+ spin-orbit split doublet in Fig. 1(a), the N_2^+ and $\text{NO}^+(\text{}^1\Pi, \text{}^3\Pi)$ ionization peaks in Fig. 1(c), and H_2O^+ and $\text{NO}^+(\text{}^1\Pi, \text{}^3\Pi)$ features in Fig. 1(d). Other observed large and weak bands, in Fig. 1(b) at 283.9 eV, in Fig. 1(c) at 412.3 eV, and in (d) at 545.0 eV, remain unassigned. Although the feature in Fig. 1(b) might be a satellite structure (shake-up), the other bands in Fig. 1(c) and (d) seem to be too close in energy for the main ionization line to be shake-up satellites, and are not compatible with IP values of small molecules containing N and O atoms as N_2O or NO_2 . Further experimental and theoretical work is needed to conclusively assign these low intensity bands.

The theoretical IP values are presented in Table 1 together with the experimental values and a previous theoretical prediction,⁶ based on a ground state HF calculation relying on the Koopmans' theorem approximation, that neglects both electron correlation and relaxation effects. The experimental and theoretical IP values agree reasonably well. The differences in the IP values obtained by the ΔHF and the ΔDFT methods are, in general, smaller than about 1 eV, with the exception of the $\text{Cl } 2s$ IP where the disagreement is quite significant. Such a result could, in principle, be ascribed to electron correlation effects that can easily lead to satellites and violate the single-hole description of the ionization process for an inner-valence shell.^{48,49} The rather poor ΔDFT results reported in Table 1 for the $\text{Cl } 2s$ IP have been confirmed by similar calculations performed by using DALTON and different density functionals (B3LYP, LB94, CAMB3LYP) both for ClNO and the other two test molecules Cl_2CH_2 and ClCH_3 . The computed value was in all cases more than 10 eV below the experimental value. To improve the theoretical description of $\text{Cl } 2s$ ionization, the calculations were also performed by the higher level ΔMCSCF method. The ΔMCSCF IP value is in excellent agreement with the experiment (considering that relativistic effects are neglected) and significantly differs from the ΔDFT results. Furthermore, it is surprisingly close to the ΔHF value, which indicates a similar contribution of the

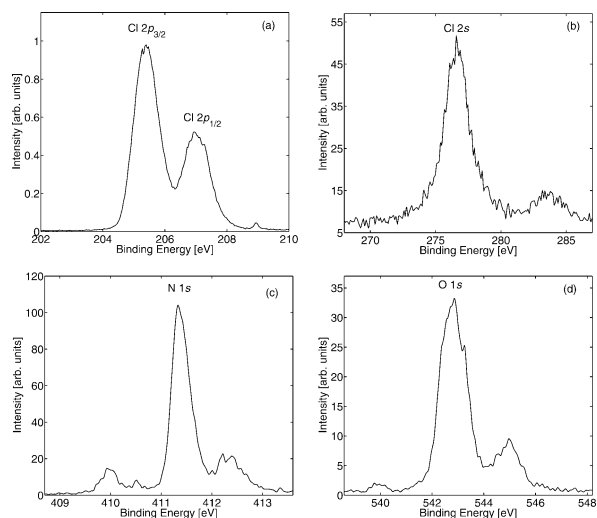


Fig. 1 The measured XPS spectra of ClNO at the photon energies of 255 eV (a), 350 eV (b), 495 eV (c), and 628 eV (d).

Table 1 Theoretical and experimental vertical IPs (eV) of ClNO

	Cl 2p _x	Cl 2p _y	Cl 2p _z	Cl 2s	N 1s	O 1s
ΔHF	206.48	206.56	206.48	276.31	412.42	542.84
ΔDFT^a	205.76	206.46	205.90	263.52	412.17	543.49
ΔDFT^b	205.47	206.26	205.70	263.27	411.57	542.84
ΔMCSCF				275.97		
Exp. ^c	206.94 ^d	205.40 ^e		276.6	411.3	542.9
	± 0.1	± 0.1		± 0.3	± 0.1	± 0.2
Theory ^f	216.0	215.9	215.9	298.1	432.6	566.6

^a Using BE88 + PD86 as exchange–correlation functional. ^b Using PBE + PBE as exchange–correlation functional. ^c Vertical IPs measured with an accuracy denoted as errors. ^d $\text{Cl } 2p_{1/2}$. ^e $\text{Cl } 2p_{3/2}$. ^f From ref. 6.

electron correlation energy both to the ground state and to this specific ionized state.

A significant error (>10 eV) in the value of the Cl 2s IP provided by the Δ DFT method is a bit surprising because this method has been successfully applied (deviations from the experimental values around 1 eV), by us (V.C.) and by several other research groups, for the calculation of core IPs of atoms such as C, N, O, F in a wide variety of molecules. To the best of our knowledge, the present calculations are the first documented application of the Δ DFT approach to the $n = 2$ shell of a second-row atom. A not *ab initio* method such as DFT may present unexpected problems in calculating properties for which the density functional has not been particularly optimized.⁵⁰ An insight into the origin of

the problem is gained by comparison of the Cl 2p and Cl 2s orbital energies in the molecular ground state; they provide, according to the Koopman's theorem (KT), a frozen orbital approximation to the IPs. This approximation is afflicted, in the DFT framework, by the additional, in comparison to HF, so-called self-interaction error.⁵¹ In the HF calculation the deviation of the KT IPs from the experimental IPs has, for both Cl 2p and Cl 2s, approximately the same value ($+10$ eV) and is largely remedied by an opposite correction, again similar in value for both the ionic states, due to the electronic relaxation included in the Δ HF method. Also in the DFT framework the electronic relaxation contribution is, as it could be expected, similar for the two IPs. However, while the deviation of the KT IP supplied by the Kohn–Sham (KS)

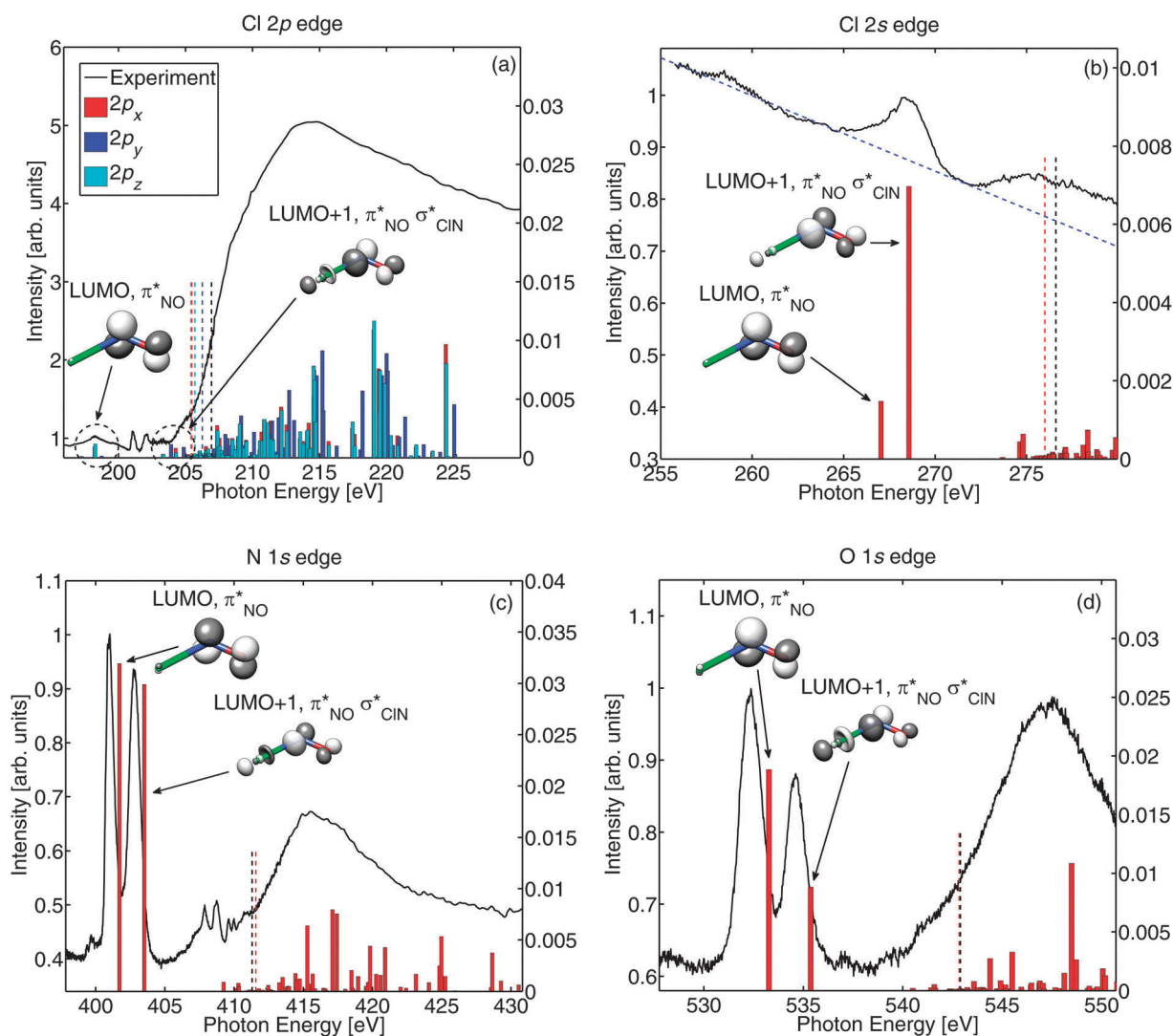


Fig. 2 The Cl 2p, Cl 2s, N 1s, and O 1s NEXAFS spectra of ClNO are presented in (a)–(d) subplots, respectively. The experimental data are shown as solid black lines. The theoretical absorption spectra obtained by the DFT transition state approximation with PBE + PBE as the exchange–correlation functional are presented by bars. The colored vertical dashed lines point to the computed ionization thresholds and the black dashed lines show the experimental IP values. In subplot (a) the gray and black dashed lines represent the experimental IP values for Cl 2p_{3/2} and Cl 2p_{1/2} levels, respectively. The molecular excited orbitals associated with the resonances are shown as inserts in the figure. In the inserts, bonds associated with Cl, N, and O are depicted in green, blue, and red, respectively. For the Cl 2s edge shown in subplot (b) the theoretical predictions are shifted by 12.5 eV, which is the difference between the Δ DFT IP value and the more accurate Δ MCSF one. In the same subplot the dashed blue line roughly approximates the monotonic contribution from the Cl 2p ionization continua.

orbital eigenvalue for Cl 2p is about -9 eV, in the case of Cl 2s it is as large as -19 eV. The significant deviation of the Δ DFT Cl 2s IP then finally derives from the unsatisfactory KS eigenvalue of the Cl 2s orbital that could be more sensitive to the self-interaction error.

The presently observed anomalous behavior of the Δ DFT method needs a thorough and extensive investigation that, however, is outside the scope of the present work. Here we only report the observation of an anomalous behavior of the Δ DFT method for the Cl 2s IP and show that this occurs for several density functionals and different codes so that it can actually be considered as a limitation of the method, at least when applied using the usually employed density functionals.

It should be noted that the theoretical IPs of the Cl 2p edge have been obtained in the non-relativistic approximation, neglecting the spin-orbit coupling which gives rise to an energy splitting that, from the experimental spectrum, can be estimated to be 1.54 eV. The calculated Cl 2p IPs take into account, instead, the splitting of the “atomic-like” 2p shell levels by the molecular field. Such energy splitting, which is predicted to lie in the range of 0.1 eV (Δ SCF)–0.5 eV (Δ DFT), is, of course, a further contribution to the broadening of the Cl 2p bands.

4.2 NEXAFS data

The experimental NEXAFS spectra of ClNO recorded at the four edges, Cl 2p, Cl 2s, N 1s, and O 1s, are shown as solid lines in Fig. 2(a)–(d), respectively. In the same figures, the bar diagrams present the theoretically predicted NEXAFS spectra, and vertical dashed lines pointing to the photon energy axis show the experimental and theoretical IP values (Table 1). Table 2 summarizes the theoretical excitation energies of core electrons to the LUMO and LUMO + 1 obtained by the DFT transition state approximation. As expected, the computed spectra have a small dependence on the chosen density functional, essentially only a small energy shift clearly related to the different predicted values of the ionization threshold (see Table 1). It should be mentioned that the Cl 2s NEXAFS spectrum was more difficult to record than the other spectra because of a rather relatively small contribution of Cl 2s excitation processes to the total photoabsorption cross section in the energy range investigated. At 280 eV photon energy, for instance, the contribution of Cl 2s ionization can be approximately derived from Fig. 2(b) as 8% of the total ion signal. This estimate is in reasonably good agreement with the ratio between the Cl 2s and the total

ionization cross sections theoretically calculated at 280 eV for the Cl atom as 11%.⁵²

4.2.1 Nitrogen and oxygen K-edge NEXAFS. The experimental NEXAFS spectra at the nitrogen and oxygen K-edges (Fig. 2(c) and (d)) show two distinct sharp features and a broad band located above the ionization thresholds, the so-called shape-resonance.¹⁵ The two bands in the N 1s spectrum, observed at 401.03 eV and 402.73 eV, are followed by a broad band with a maximum at 415.5 eV. The corresponding sharp features in the O 1s spectrum are detected at 532.37 eV and 534.62 eV, while the shape resonance structure is centered approximately at 547 eV. A comparison of the experimental data and theoretical predictions (Fig. 2(c) and (d)) enabled us to assign the lowest two bands for the N and O K-edges to $1s \rightarrow \pi_{\text{NO}}^*$ and $1s \rightarrow \sigma_{\text{CIN}}^* \pi_{\text{NO}}^*$ excitation transitions, respectively. The excited molecular orbitals associated with these transitions, which are depicted in the figures, imply that the LUMO π^* orbital is orthogonal to the molecular plane and localized on the N and O atoms, while the LUMO + 1 antibonding orbital is located in the molecular plane and is represented by both π_{NO}^* and σ_{CIN}^* characters. This is similar to the assignment of the excitations in the UV-visible absorption spectrum.^{8,9} It is worth noting that core-valence excitations in NEXAFS spectra, at variance with electron excitations in the UV-visible absorption spectroscopy, can directly probe with atomic selectivity delocalization properties of empty MOs. In the present case, for instance, a large difference is observed in the LUMO/LUMO + 1 intensity ratio of the two lowest lying resonances on going from the N 1s spectrum to the O 1s one. This ratio is close to one for the N 1s core-hole and approximately two for the O 1s. This clearly points out the substantial decrease in the MO density at the oxygen atom of the LUMO + 1 with respect to the LUMO, whilst this change is not observed in the nitrogen atom. This can be seen by comparing the MO inserts and the theoretical intensities of Fig. 2(c) to those of Fig. 2(d) for the two transitions involved. Just below the ionization N $1s^{-1}$ threshold the theory predicts weak excitations of the Rydberg character that are also in good agreement with the experiment (Fig. 2(c)). The weak features observed in the 407–410 eV range are therefore assigned to Rydberg excitations. Rydberg series below the O $1s^{-1}$ threshold are instead very weak, being barely visible in the experimental spectrum. This finding is also in agreement with the results of the calculated O 1s NEXAFS spectrum (Fig. 2(d)). The fact that excitations of this type are less intense in the O 1s absorption spectrum is generally attributed to the shorter extension of the O 1s orbital in comparison to the N 1s orbital, and hence to a reduced overlap with Rydberg orbitals.

Above the N $1s^{-1}$ and O $1s^{-1}$ ionization thresholds the theoretical intensity distribution may show a dependence on the chosen basis set and, as mentioned before, should be analyzed by a moment theory.³⁶ However, at least from a qualitative point of view, we can observe a group of strong excitations in the energy region where the experiment shows a broad intense band (shape-resonance). For the N 1s spectrum an analysis of the excited orbitals involved in this broad band shows that the most intense transition is associated with an antibonding σ^* orbital along the

Table 2 Main theoretical core excitation energies from DFT calculations in the transition state approximation using different density functionals

	Cl 2p _x	Cl 2p _y	Cl 2p _z	Cl 2s ^c	N 1s	O 1s
LUMO	196.84 ^a 196.69 ^b	197.22 ^a 197.24 ^b	196.95 ^a 196.73 ^b	266.96 ^a 267.31 ^b	402.22 ^a 401.72 ^b	533.82 ^a 533.27 ^b
LUMO + 1	198.34 ^a 198.21 ^b	198.83 ^a 198.75 ^b	198.52 ^a 198.27 ^b	268.54 ^a 268.34 ^b	404.07 ^a 403.51 ^b	535.96 ^a 535.37 ^b

^a Using BE88 + PD86 as exchange–correlation functional. ^b Using PBE + PBE as exchange–correlation functional. ^c The values were shifted by 12.5 eV (see text for explanation).

N–O bond. Higher in energy we find excitations to a sort of σ_{CIN}^* orbital that, however, has a very small contribution to the N site and therefore it is extremely weak. In the O 1s spectrum the broad shape resonance appears at around 547 eV and, similar to the case of the N K-edge, is assigned to σ_{NO}^* excitations.

The assignment for the two strong core–valence resonances below threshold in the K-edge N 1s and O 1s spectra is supported by the results of our experiment, still unpublished, and was investigated by performing 3D multiple ion momentum spectroscopy of the $\text{Cl}^+/\text{N}^+/\text{O}^+$ fragmentation channel at the two resonance energies in both NEXAFS spectra. A remarkably different molecular alignment is observed depending on the nature of the excitation involved, being connected to the transition moment vector which either lies on the molecular plane or is perpendicular to it.

4.2.2 Chlorine L-edge NEXAFS. The NEXAFS spectra of the chlorine L-edge of ClNO are shown in Fig. 2(a) and (b). Although the N and O K-edge spectra of ClNO exhibit a typical intensity distribution for a core NEXAFS spectrum, the spectra at the Cl L-edge are more complicated because of the more diffuse character of the holes and more relevant electron correlation effects. In the case of the $L_{2,3}$ -edge (Fig. 2(a)) the calculations have been performed for the 3 components of the 2p shell, *i.e.*, including the molecular field splitting but neglecting the spin–orbit coupling effect. The latter is particularly important for the energy region below the ionization threshold, where relatively narrow bands may be found, and is sometimes included empirically by using known values of spin–orbit energy splitting. This splitting, as mentioned before, has been found in the present XPS investigation as 1.54 eV. In the continuum, however, inclusion of such empirical splitting would, of course, be meaningless considering that a NEXAFS spectrum generally shows only very broad unresolved bands above the threshold. In the present case it does not appear necessary to apply any correction because the main characteristics of the spectral distribution are already described by the presently adopted approximations. The calculations performed for the $L_{2,3}$ -edge (Fig. 2(a)) predict very weak excitations below the ionization threshold, which is in good agreement with the experimental data. Most of the Cl 2p excited states that significantly contribute to the spectrum have a continuum character (scattering states), *i.e.*, they are located above the threshold, while the ones with a “quasi-bound” character and located below the threshold are only slightly populated due to photon absorption. This can be ascribed to the more diffuse L hole in comparison with a K hole, which affects the value of the transition moment and also reduces the “attractive power” of the more diffuse L hole charge. A close inspection at low energies of the experimental spectrum of Fig. 2(a) points out the weak and broad absorption of the lowest lying resonances. These unresolved transitions exhibit the spin–orbit split and the relative intensities of the two components observed in the Cl 2p XPS spectrum (Fig. 1(a)). The most intense component of the doublet is located at 198.20 eV. These features are ascribed to the group of excitations to the LUMO (π^*), which are split by the molecular field and the spin–orbit interaction. This finding is in excellent agreement with the theoretical results, where the spin–orbit effect is not taken into account.

The experimental Cl 2s NEXAFS spectrum of ClNO exhibits a rather weak, broad and asymmetric peak centered at 268.5 eV. This is assigned to transitions to the LUMO and the LUMO + 1, with rather different intensities, embedded in a strong continuous contribution, originating from the Cl 2p ionization processes, which is designated in Fig. 2(b) as a broken line. According to the previous discussion on the IP calculations, the best prediction for the Cl 2s ionization is 276 eV, as obtained by the ΔMCSCF model. This theoretical value is in good agreement with the experimental value of 276.6 eV. The Cl 2s NEXAFS spectrum was calculated by the ΔDFT method which does not accurately predict the Cl 2s ionization threshold. The difference in the Cl 2s IP obtained by the two methods, ΔMCSCF and ΔDFT , is 12.5 eV; we applied it as an energy shift to the ΔDFT Cl 2s NEXAFS spectrum. This procedure enables us to assign the experimentally measured NEXAFS peak to the closely lying LUMO and LUMO + 1 excitations that could not be experimentally resolved due to the large Cl 2s core-hole lifetime broadening and the interaction with the continuum background. Similar to the assignments at the other three edges, the LUMO and LUMO + 1 at the Cl 2s edge have the out-of-plane π_{NO}^* and in-plane $\sigma_{\text{CIN}}^*\pi_{\text{NO}}^*$ character, respectively.

5 Conclusions

We reported experimental ClNO XPS spectra from which we calculated the Cl 2p, Cl 2s, N 1s, and O 1s binding energies, as well as ClNO NEXAFS spectra recorded in the vicinity of the same edges. We also performed theoretical calculations with different levels of accuracy to predict the IP values and to assign the NEXAFS features in the experimental spectra. Most of the binding energy calculations were performed by ΔHF and ΔDFT methods while the absorption spectra have been calculated by the DFT method in the transition state approximation.

The theoretical results enabled us to assign most of the features observed in the experimental absorption spectra. Similar intensity patterns are observed for the K-edge NEXAFS spectra of the N and O light atoms. This is a generally observed pattern in spectra of molecules containing first-row atoms. At variance with the case of the K-shell, absorption spectra of excitations from the L-shells of the second-row Cl atom (Cl 2s and Cl 2p) exhibit distinctively different patterns. In the case of Cl 2p, almost all the oscillator strength is observed in the ionization continua (inner shell excitations above the ionization thresholds), and the “quasi-discrete” core–valence excitations display very small relative intensities. In the case of the Cl 2s NEXAFS, the intensity pattern is dominated by the underlying manifold of Cl 2p ionization continua, and the Cl 2s excitations are weak and characterized by a very large core-hole lifetime broadening due to the fast Koster–Cronig decay processes.

Apart from the Cl 2s, the theoretical IP values agree reasonably well with the experimental ones. To improve the agreement also for the Cl 2s IP we have adopted a higher level of theory, namely the ΔMCSCF method, that predicts an IP that is very close to the experimental value. The comparison of the

Cl 2s and Cl 2p IP values calculated by the Δ HF and Δ DFT methods in ClNO points out an anomalous behavior of the DFT approach for the Cl 2s IP. A significant deviation of the Δ DFT IP value derives from the unsatisfactory KS eigenvalue of the Cl 2s orbital that could be more sensitive to the self-interaction error. Although this observation deserves an extensive investigation for a deeper understanding, the anomalous behavior occurs for several density functionals and different codes. It therefore seems to be a limitation of the method, at least when it is applied using the usually employed density functionals.

The theoretical assignment of the NEXAFS features suggest that the LUMO and the LUMO + 1 in the NEXAFS spectra at the four edges are similar to the LUMO and LUMO + 1 in the ground state, *i.e.*, they have the out-of-plane π_{NO}^* and in-plane $\sigma_{\text{CIN}}^* \pi_{\text{NO}}^*$ character, respectively. Our calculations also reveal a clear localization of the LUMO along the N–O bond (Fig. 2), suggesting that by a selective excitation of this resonance, the cleavage of this bond could be preferentially activated.

Acknowledgements

This work was financially supported by the Swedish Research Council (VR) and the Knut and Alice Wallenberg Foundation, Sweden. C.L. and V.C. are grateful for the contribution of the “Ministero della Istruzione della Università e della Ricerca, Direzione Generale per la Internazionalizzazione della Ricerca” of the Republic of Italy and for the partial support of PRIN 2010ERFKXL. The authors would like to thank the referees for their valuable comments and suggestions. The authors also acknowledge the open access contribution of the Research Infrastructure (RI) Elettra.

References

- R. Karlsson and E. Ljungström, *Atmos. Environ.*, 1998, **32**, 1711.
- B. J. Finlayson-Pitts, *Chem. Rev.*, 2003, **103**, 4801.
- G. Cazzoli, C. Degli Esposti, P. Palmieri and S. Simeone, *J. Mol. Spectrosc.*, 1983, **97**, 165.
- D. C. Frost, S. T. Lee, C. A. McDowell and N. P. C. Westwood, *J. Electron Spectrosc. Relat. Phenom.*, 1975, **7**, 331.
- M. I. Abbas, J. M. Dyke and A. Morris, *J. Chem. Soc., Faraday Trans. 2*, 1976, **72**, 814.
- E. Gilberg, W. Schätzl and H. W. Schrenk, *Chem. Phys.*, 1976, **13**, 115.
- The MO numbering adopted in the present paper takes into account all electrons and symmetries, discriminating between a' and a'' irreducible representations.
- Y. Y. Bai, A. Ogai, C. X. W. Qian, L. Iwata, G. A. Segal and H. Reisler, *J. Chem. Phys.*, 1989, **90**, 3903.
- C. X. W. Qian, A. Ogai, J. Brandon, Y. Y. Bai and H. Reisler, *J. Phys. Chem.*, 1991, **95**, 6763.
- V. Skorokhodov, Y. Sato, K. Suto, Y. Matsumi and M. Kawasaki, *J. Phys. Chem.*, 1996, **100**, 12321.
- S. Lacombe, M. Loudet, A. Dargelos and J. M. Camou, *Chem. Phys.*, 2000, **258**, 1.
- J. L. Mackey, B. R. Johnson, C. Kittrell, L. D. Le and J. L. Kinsey, *J. Chem. Phys.*, 2001, **114**, 6631.
- T. Yamashita and S. Kato, *J. Chem. Phys.*, 2004, **121**, 2105.
- K. M. Jones, J. A. Milkiewicz, B. J. Whitaker, A. G. Sage and G. A. Worth, *ChemPhysChem*, 2013, **14**, 1479.
- J. Stöhr, in *NEXAFS Spectroscopy, Springer Series in Surface Sciences 25*, ed. S. G. Erti, R. Gomer and D. L. Mills, Springer-Verlag, Berlin, Heidelberg, New York, 1992.
- C. L. Yaws, *Chemical Properties Handbook*, McGraw-Hill, 1999.
- encyclopedia.airliquide.com.
- J. M. Dyke, D. Haggerston, A. Morris, S. Stranges, J. B. West, T. G. Wright and A. E. Wright, *J. Chem. Phys.*, 1997, **106**, 821.
- R. R. Blyth, R. Delaunay, M. Zitnik, J. Krempasky, R. Krempaska, J. Slezak, K. C. Prince, R. Richter, M. Vondracek, R. Camilloni, L. Avaldi, M. Coreno, G. Stefani, C. Furlani, M. de Simone, S. Stranges and M.-Y. Adam, *J. Electron Spectrosc. Relat. Phenom.*, 1999, **101–103**, 959.
- G. Johansson, J. Hedman, A. Berndtsson, M. Klasson and R. Nilsson, *J. Electron Spectrosc. Relat. Phenom.*, 1973, **2**, 295.
- T. D. Thomas, *J. Am. Chem. Soc.*, 1970, **92**, 4184.
- M. Thompson, P. A. Hewitt and D. S. Wooliscroft, *Anal. Chem.*, 1978, **50**, 690.
- E. J. Aitken, M. K. Bahl, K. D. Bomben, J. K. Gimzewski, G. S. Nolan and T. D. Thomas, *J. Am. Chem. Soc.*, 1980, **102**, 4873.
- A. P. Hitchcock and C. E. Brion, *J. Electron Spectrosc. Relat. Phenom.*, 1980, **18**, 1.
- M. Tronc, G. C. King and F. H. Read, *J. Phys. B: At. Mol. Phys.*, 1979, **12**, 137.
- G. C. King, M. Tronc, F. H. Read and R. C. Bradford, *J. Phys. B: At. Mol. Phys.*, 1997, **10**, 2479.
- M. W. Schmidt, K. K. Baldridge, J. A. Boatz, S. T. Elbert, M. S. Gordon, J. J. Jensen, S. Koseki, N. Matsunaga, K. A. Nguyen, S. Su, T. L. Windus, M. Dupuis and J. A. Montgomery, *J. Comput. Chem.*, 1993, **14**, 1347.
- T. H. Dunning, *J. Chem. Phys.*, 1971, **55**, 716.
- Dalton, a molecular electronic structure program*, <http://daltonprogram.org>.
- K. Hermann, L. G. M. Pettersson, M. E. Casida, C. Daul, A. Goursot, A. Koester, E. Proynov, A. St-Amant and D. R. Salahub with contributions from V. Carravetta, H. Duarte, C. Friedrich, N. Godbout, J. Guan, C. Jamorski, M. Leboeuf, M. Leetmaa, M. Nyberg, S. Patchkovskii, L. Pedocchi, F. Sim, L. Triguero and A. Vela, *StoBe-deMon version 3.0*, 2007.
- W. Kutzelnigg, U. Fleischer and M. Schindler, *NMR-Basic Principles and Progress*, Springer-Verlag, Heidelberg, 1990, vol. 23, p. 165.
- http://www.demon-software.com/public_html/support/html/ug-node116.html.
- A. D. Becke, *Phys. Rev. A: At., Mol., Opt. Phys.*, 1988, **38**, 3098.
- J. P. Perdew, *Phys. Rev. B: Condens. Matter Mater. Phys.*, 1986, **33**, 8822.
- J. P. Perdew, K. Burke and M. Ernzerhof, *Phys. Rev. Lett.*, 1996, **77**, 3865.

- 36 P. W. Langhoff, C. T. Corcoran, J. S. Sims, F. Weinhold and R. M. Glover, *Phys. Rev. A: At., Mol., Opt. Phys.*, 1976, **14**, 1042.
- 37 V. Carravetta and H. Ågren, *Computational Strategies for Spectroscopy*, Wiley Online Library, 2012, p. 137.
- 38 L. Triguero, L. G. M. Pettersson and H. Ågren, *Phys. Rev. B: Condens. Matter Mater. Phys.*, 1998, **58**, 8097.
- 39 P. Bolognesi, P. O'Keeffe, Y. Ovcharenko, M. Coreno, L. Avaldi, V. Feyer, O. Plekan, K. C. Prince, W. Zhang and V. Carravetta, *J. Chem. Phys.*, 2010, **133**, 34302.
- 40 L. Yang, H. Ågren, V. Carravetta and L. G. M. Pettersson, *Phys. Scr.*, 2006, **54**, 614.
- 41 I. Hjelte, O. Bjorneholm, V. Carravetta, C. Angeli, R. Cimiraglia, K. Wiesner, S. Svensson and M. N. Piancastelli, *J. Chem. Phys.*, 2005, **123**, 64314.
- 42 T. D. Thomas, *J. Am. Chem. Soc.*, 1970, **92**, 4184.
- 43 C. Nicolas and C. Miron, *J. Electron Spectrosc. Relat. Phenom.*, 2012, **185**, 267.
- 44 T. Hatamoto, M. Matsumoto, X. J. Liu, K. Ueda, M. Hoshino, K. Nakagawa, T. Tanaka, H. Tanaka, M. Ehara, R. Tamaki and H. Nakatsuji, *J. Electron Spectrosc. Relat. Phenom.*, 2007, **155**, 54.
- 45 U. Hergenhahn, *J. Phys. B: At., Mol. Opt. Phys.*, 2004, **37**, R89.
- 46 X. J. Liu, G. Prumper, F. Gel'mukhanov, N. A. Cherepkov, H. Tanaka and K. Ueda, *J. Electron Spectrosc. Relat. Phenom.*, 2007, **156**, 73.
- 47 U. Hergenhahn, O. Kugeler, A. Rudel, E. E. Rennie and A. M. Bradshaw, *J. Phys. Chem. A*, 2014, **105**, 5704.
- 48 L. S. Cederbaum, G. Hohlneicher and W. V. Niessen, *Mol. Phys.*, 1973, **26**, 1405.
- 49 V. Carravetta and R. Moccia, *Mol. Phys.*, 1978, **35**, 129.
- 50 P. Verma and R. J. Bartlett, *J. Chem. Phys.*, 2014, **140**, 18A534.
- 51 G. Tu, V. Carravetta, O. Vahtras and H. Ågren, *J. Chem. Phys.*, 2007, **127**, 174110.
- 52 J. J. Yeh and I. Lindau, *At. Data Nucl. Data Tables*, 1985, **32**, 1.